NANO · MICRO small
www.small-journal.com

Nanoengineered Organic Electrodes for Highly Durable and Ultrafast Cycling of Organic Sodium-Ion Batteries

*Ranjith Thangavel, Megala Moorthy, Bala Krishnan Ganesan, Wontae Lee, Won-Sub Yoon, and Yun-Sung Lee**

Sodium-ion batteries (SIBs) have become increasingly important as next-generation energy storage systems for application in large-scale energy storage. It is very crucial to develop an eco-friendly and green SIB technique with superior performance for sustainable future use. Replacing the conventional inorganic electrode materials with green and safe organic electrodes will be a promising approach. However, the poor electrochemical kinetics, unstable electrode–electrolyte interface, high solubility of the electrodes in the electrolyte, and large amount of conductive carbon present great challenges for organic SIBs. In this study, the issues of organic electrodes are addressed through atomic-level manipulation of these organic molecules using a series of ultrathin (Å-level) metal oxide coatings (Al_2O_3, ZnO, and TiO_2). Uniform and precise coatings on the perylene-3,4,9,10-tetracarboxylicacid dianhydride by gas-phase atomic layer deposition technique shows a stable interphase, enhanced electrochemical kinetics (71C, 10 A g^{-1}), and excellent stability (89%–500 cycles) compared to conventional organic electrode (70%–200 cycles). Further studies reveal that the chemical stability of the metal oxide coating layer plays a critical role in influencing the redox behavior, and improving kinetics of organic electrodes. This study opens a new avenue for developing high-energy organic SIBs with performance equivalent to inorganic counterparts.

1. Introduction

The demand for high-performance energy storage devices is rapidly increasing to meet the requirements of next-generation applications such as large-scale storage grids and electric vehicles. Currently, Li-ion battery (LIB) technologies dominate the portable electronics market and have begun to be successfully applied in commercial electric and hybrid electric vehicles. However, the increasing market demand for rechargeable LIBs has increased the concerns regarding the economic sustainability of the LIB technology owing to uneven geographical distribution and relatively low amount of available lithium resources.[1–3] Thus, battery technologies based on abundant and inexpensive resources shall be an important option for large-scale energy storage devices.

In this context, sodium-ion battery (SIB) technologies have emerged as a promising and low-cost alternative to LIBs. An intercalation-based chemical mechanism, similar to that of their LIB counterparts, wide sodium resource availability, and excellent electrochemical performance make SIBs an attractive candidate technology for large-scale storage devices. A variety of electrode materials such as layered oxides, polyanions, and fluorophosphates were successfully studied as cathodes for SIBs.[4,5] Although graphite does not offer a favorable Na^+ intercalation chemistry, several metal sulfides, metals, phosphides, alloys, and hard carbon were investigated as anodes for SIBs.[6–8] The limited capacity of metal oxides, poor cycle life, high cost of hard carbon, and large volume expansion of alloy/metal type anodes limit their practical application.[9,10] Transferring the experience gained from current LIBs to SIBs may lead to the rapid commercialization of the SIB technology.

The most studied electrode materials in both LIBs and SIBs are based on transition metal-based chemistries using metal elements that are generally nonrenewable resources. Furthermore, the highly toxic nature of transition metals and high energy consumption involved in metal mining must be addressed to increase the sustainability and environment friendliness of energy storage devices.[11–13] Organic materials are promising candidates for further advancing the sustainability and eco-friendliness of energy storage devices. Organic electrode materials offer many advantages because they mostly consist of light elements such as C, H, O, N, and S. First, organic electrode materials are directly available from natural resources or can be prepared from natural derivatives.[14,15] Organic electrodes have good structural flexibility and wide chemical diversity; further, they can provide a high specific capacity and high voltage at low

Dr. R. Thangavel, M. Moorthy, B. K. Ganesan, Prof. Y.-S. Lee
School of Chemical Engineering
Chonnam National University
Gwangju 61186, Republic of Korea
E-mail: leeys@chonnam.ac.kr

Dr. R. Thangavel, Dr. W. Lee, Prof. W.-S. Yoon
Department of Energy Science
Sungkyunkwan University
Suwon 440-746, Republic of Korea

Dr. W. Lee
The Institute of New Paradigm of Energy Science Convergence
Sungkyunkwan University
Suwon 16419, Republic of Korea

The ORCID identification number(s) for the author(s) of this article can be found under https://doi.org/10.1002/smll.202003688.

DOI: 10.1002/smll.202003688

cost with an appropriate molecular design.[16,17] Recently, it was demonstrated that organic electrode materials outperform their inorganic counterparts in terms of energy, power, and cycle life.[18–20]

Electroactive organic electrodes are primarily classified into i) p-type electrodes that donate electrons from their neutral state to undergo oxidation, ii) n-type electrodes that accept electrons to undergo reduction, and iii) bipolar type electrodes that are capable of undergoing both oxidation and reduction from the neutral state. The redox centers that are abundant and widely available in organic electrodes are the active sites for Na^+ storage. The storage reaction mechanisms in all electroactive organic materials are mostly based on carbonyl reactions (C=O), doping reactions, and C=N reactions.[21–23]

While highly advantageous, organic electrodes face several critical problems owing to their poor electronic conductivity and very low cycle life. Organic electrodes have wide bandgaps, and thus, they feature very low electronic conductivity, leading to a poor rate performance. A large amount of conductive carbon additives (nearly 50 wt%) such as carbon nanotubes, ketjen black, and graphene oxide have been used to enhance the kinetics of organic electrodes.[24–26] However, the use of such strategies inevitably degrades the overall energy density of the system due to the presence of a large amount of electrochemically inactive material. While molecular-level tailoring and nanostructuring of the organic electrodes have been proven to improve the rate characteristics, these techniques cannot be adopted for all organic materials.[27–30]

The low cyclability of organic electrodes is attributed to the high solubility of small organic molecules in aprotic organic electrolytes. The organic electrolytes can easily solvate small organic molecules and induce electrode dissolution upon continuous cycling, thereby reducing the cycle life of organic electrodes.[31,32] Approaches such as the infiltration of organic molecules in high-surface-area carbon, use of suitable electrolyte and additives, and polymerization of small molecules have been pursued in previous studies to improve the cycle life.[33,34] However, these approaches can result in a poor rate performance and reduce the energy density owing to the increase in the electrode material weight. Thus, a simple method addressing the aforementioned issues is urgently required to achieve high-performing organic electrodes with high rate performance and enhanced durability.

In this study, we address the problematic solubility and kinetics of organic electrodes through atomic-level manipulation of the organic electrode particles using an ultrathin metal oxide coating. Metal oxide coatings are well known to improve the kinetics and cycle life of the inorganic electrodes by preventing the dissolution of the active material into the electrolyte and by increasing the ion-diffusion kinetics. Coatings based on several metal oxides such as TiO_2, ZnO, Al_2O_3, and ZrO_2 were successfully employed over several inorganic anodes and cathodes for application in Li-ion and Na-ion batteries. However, this strategy has not been implemented to improve the performance of organic electrodes. Conventional metal oxide coating methods (solid-state, sol–gel, and hydrothermal) involve the use of high-temperature processes that are not suitable for organic electrodes owing to their low thermal stability.[35] Furthermore, uniform, precise, and ultrathin coatings cannot be realized with conventional techniques. Recently, atomic layer deposition (ALD) has emerged as an attractive tool for obtaining ultrathin (Å-level) metal oxide coatings via gas phase reactions at a very low temperature.[36,37] Highly tunable, highly pure, conformal coatings can be easily deposited with ALD. In particular, ALD has been recently successfully used for advanced energy storage systems such as sulfur batteries, metal batteries, and solid-state batteries.[37–39] Nevertheless, the application of ALD for organic electrodes of SIBs has been limited. Here, we analyze the effect of several metal oxides (Al_2O_3, ZnO, and TiO_2) coated on the perylene-3,4,9,10-tetracarboxylicacid dianhydride (PTCD) organic electrode. Recently, PTCD has emerged as a great choice of electrode for organic SIBs because of its multiple redox sites, which delivers a high capacity. The sodium ions can be stored into the aromatic rings by a simple enolation reaction at carbonyl group (C=O) with no structural expansion.[40] The commercial availability of PTCD could greatly encourage the practical implementation of organic SIBs. The influence of metal oxide coatings on the electrochemical performance is studied, and it is established that the surface-engineered organic electrode features higher stability and superior rate performance, compared to the non-coated organic electrodes. The present study will enable the emergence of highly sustainable energy storage devices with superior performance.

2. Results and Discussion

Commercial PTCD obtained from the vendor was used for the experiments. X-ray diffraction (XRD) patterns of the pristine PTCD presented in **Figure 1**a indicate the crystalline nature of the electrode materials with a monoclinic structure (β-form) and the $P21/c$ space group. The XRD patterns of the ZnO-, Al_2O_3-, and TiO_2-coated PTCD powders exhibit no additional peaks associated with metal oxides, indicating the ultrathin and amorphous nature of the coating layer over PTCD particles.[41,42] As illustrated in Figure 1b, the chemical structure of PTCD is conjugated with a stable aromatic core containing four carbonyl groups that can exhibit stable sodium-ion storage behavior.[43,44] The electrochemically active carboxylic groups act as the Na-ion storage sites through the enolation process.[45]

Scanning electron microscope (SEM) images of PTCD in Figure S1 in the Supporting Information revealed the rod-like morphology, formed by agglomeration of micrometer-sized particles. Figure 1c–e presents the high-resolution transmission electron microscopy (HR-TEM) images of PTCD coated with 50 cycles of metal oxide ALD. Studying the thickness of ALD coating obtained using a low number of ALD cycles is fairly difficult, and therefore, the PTCD samples coated with 50 cycles are used here. A uniform amorphous metal oxide coating is formed over the particle after the ALD process, with coating thicknesses of ≈6.85, 6.35, and 6.38 nm for Ti-PTCD, Al-PTCD, and Zn-PTCD, respectively. The growth rates of TiO_2, Al_2O_3, and ZnO over PTCD were ≈1.37, 1.27, and 1.28 Å per cycle, respectively, and it can be concluded that 2 cycles of TiO_2, Al_2O_3, and ZnO ALD coating on PTCD result in coating thicknesses of ≈2.74, 2.54, and 2.56 Å, respectively. Conventional metal oxide coating techniques (solid-state, sol–gel, and hydrothermal) involve high-temperature processes that are

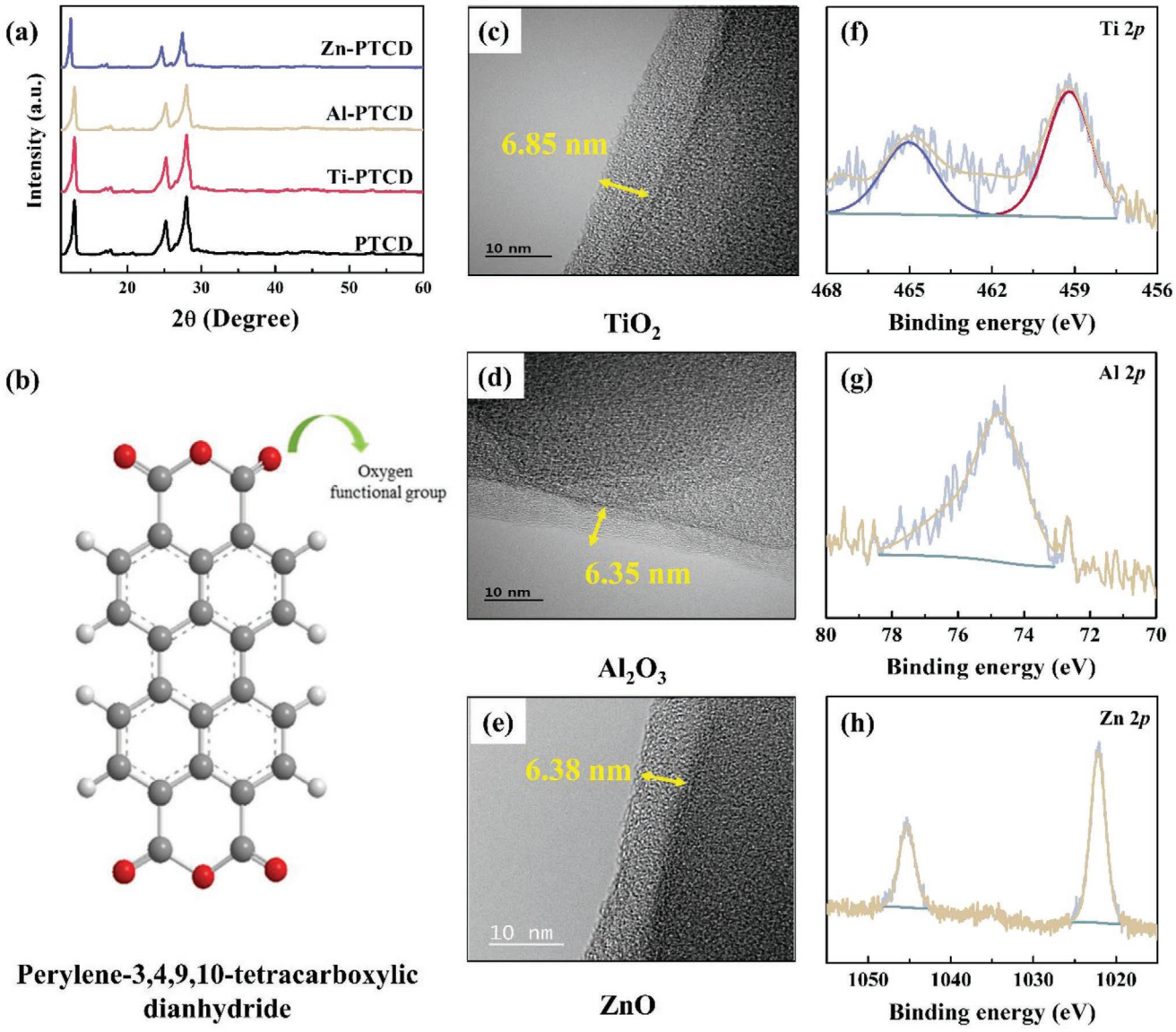

Figure 1. a) XRD patterns of PTCD and metal oxide-coated PTCD. b) Chemical structure of PTCD. c–e) TEM images of different metal oxide-coated PTCD. f–h) Deconvoluted XPS spectra of different metal oxide-coated PTCD samples.

not suitable for organic electrodes owing to their low thermal stability.[46] In contrast, the low-temperature gas phase reactions used in the ALD process at a very low temperature enable the deposition of highly tunable, highly pure, conformal coatings on organic electrodes without affecting their chemical and physical properties.

The surface compositions of the various metal oxide coatings on the PTCD particles were further verified by X-ray photoelectron spectroscopy (XPS) analysis. The XPS spectrum of the metal oxide-coated PTCD exhibits signature peaks of corresponding metal oxides (Figure S2, Supporting Information) after the coating process. The deconvoluted Ti spectrum of Ti-PTCD (Figure 1f) exhibits doublet peaks at ≈459 and ≈465 eV, corresponding to the Ti $2p_{2/3}$ and $2p_{1/2}$ peaks, confirming the presence of TiO_2.[47,48] The XPS spectrum of Al-PTCD (Figure 1g) exhibits a peak at ≈74.5 eV that corresponds to the Al 2p peak of the Al_2O_3 coating on PTCD.[41] The Zn 2p XPS spectrum of Zn-PTCD (Figure 1h) exhibits Zn $2p_{3/2}$ and Zn $2p_{1/2}$ doublet peaks at ≈1022 and 1045 eV, respectively, confirming the presence of Zn^{2+} oxidation state of ZnO in Zn-PTCD.[49]

To explore the benefits of the metal oxide coatings over PTCD, the Na-ion storage performance was evaluated in half-cells within the potential window of 3.0–1 V at (0.1 A g^{-1}). The charge–discharge (CD) curves of pristine PTCD in **Figure 2**a (0.1 A g^{-1}) present a series of discharge plateaus between 2.5 and 2 V, indicating the sequential insertion of sodium into the carbonyl groups of PTCD to form sodium enolate. The consecutive charging process involves the desodiation of sodium enolate to form PTCD.[50] The flat plateaus during the charge and discharge process indicate that sodium-ion insertion/extraction is a two-phase reaction process.[23] The shape profiles of the first discharge and the subsequent discharge for

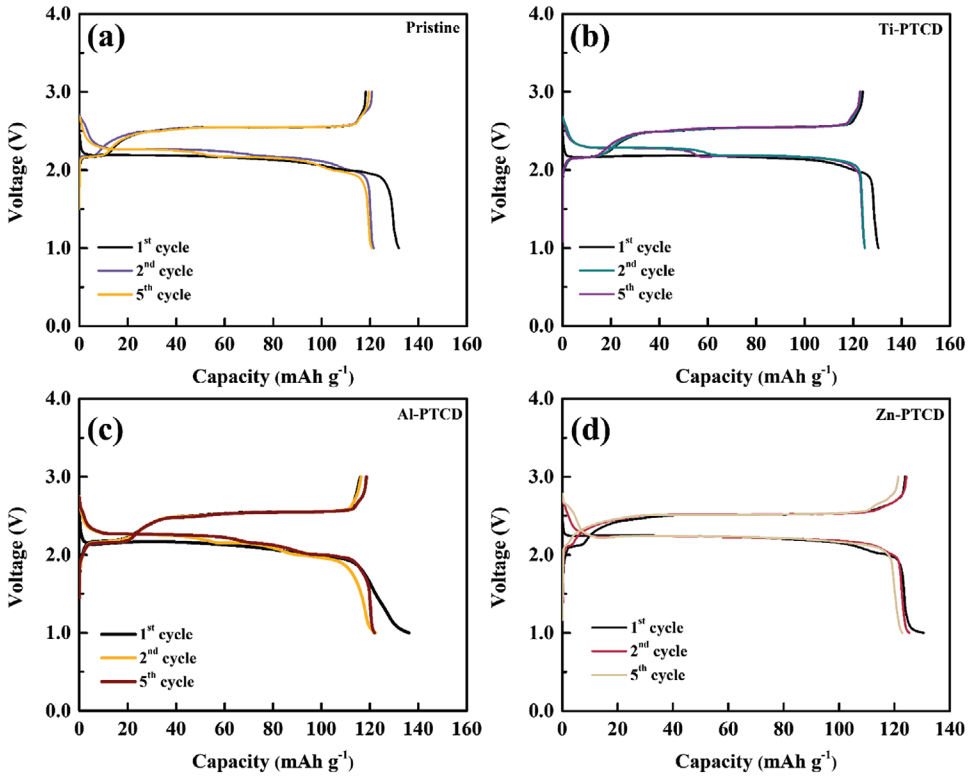

Figure 2. Charge/discharge profiles of a) pristine PTCD, b) Ti-PTCD, c) Al-PTCD, and d) Zn-PTCD.

all samples show a change due to the chemical changes in the PTCD structure, and the consecutive charge–discharge profiles remains similar thereafter. The first-cycle Coulombic efficiency of PTCD without the metal oxide coating is ≈89.3%. A low initial Coulombic efficiency is associated with irreversible capacity, originating from the unwanted electrode–electrolyte reactions of ionized sodium atoms, and the formation of a nonuniform solid electrolyte interface (SEI) layer.[51,52] A low Coulombic efficiency reduces the energy density of SIBs and presents a problematic trade-off in battery design.

The charge discharge profile of different metal oxide-coated PTCD (2 cycles of ALD) is given in Figure 2b–d. The metal oxide-coated PTCD also shows a series of flat plateaus during the charge and discharge process, indicating that metal oxides do not influence the sodium-ion storage mechanism. The metal oxide coatings strongly influence the redox potential during sodium extraction/insertion due their strong electronegativity. Compared to pristine PTCD, Ti-PTCD exhibited stable charge–discharge plateaus with negligible polarization. After coating (2 cycles of ALD), the first-cycle Coulombic efficiencies of Al-PTCD, Ti-PTCD, and Zn-PTCD were calculated as 81.8%, 95.4%, and 94.3%, respectively. This clearly reveals the facile Na^+ insertion/removal, reduced electrode–electrolyte reaction, and formation of a uniform interphase layer after the metal oxide coating. Furthermore, the polarization of the PTCD electrodes was significantly reduced after metal oxide coating for Ti-PTCD and Zn-PTCD owing to the facile Na^+ diffusion kinetics. However, the higher overpotential in Al-PTCD compared to that of bare PTCD is attributed to the sodiation process of Al_2O_3 to form a Na–Al–O complex. Although the initial sodiation process is thermodynamically unfavorable, the new sodiated layer can exhibit high Na^+ diffusivity and easily conducts Na^+ ions in subsequent cycles.[53] A similar behavior has been previously observed for other anode materials.[53] The Na^+ ion storage mechanism in PTCD organic electrode is given in **Scheme 1**.

The rate capabilities of pristine PTCD and metal oxide coatings were evaluated with the results presented in **Figure 3**a. The charge discharge profiles of pristine PTCD, and metal oxide-coated PTCD at different current rates are given in Figure S3 in the Supporting Information, and Figure 3b–d. The discharge capacity delivered by both pristine and coated PTCD is almost the same at low currents. The discharge capacities of all the

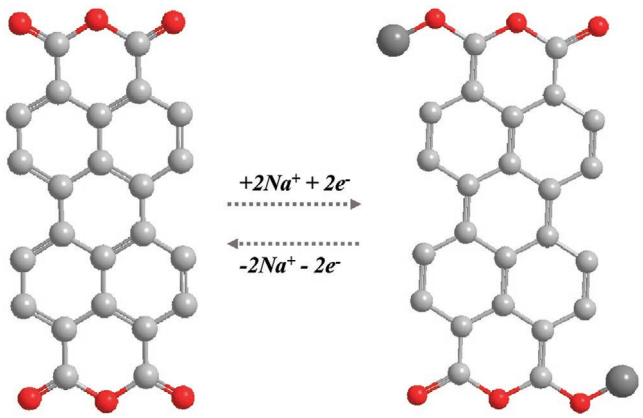

Scheme 1. Sodium-ion storage mechanism in PTCD organic molecule.

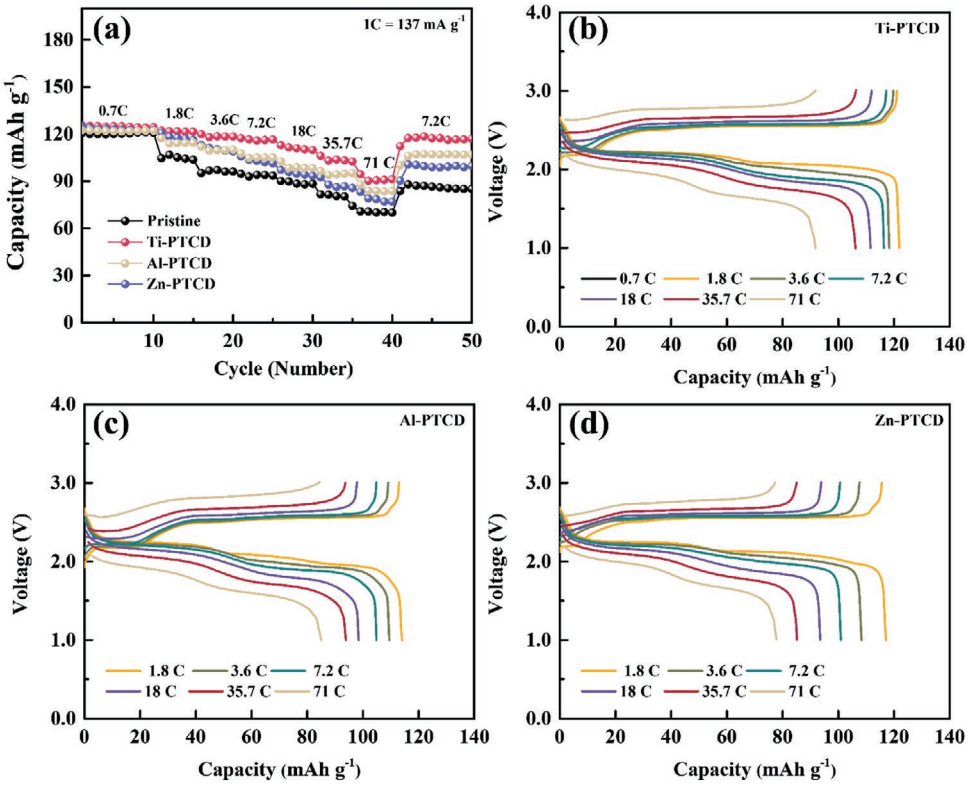

Figure 3. Effect of metal oxide coating: a) Rate performance of PTCD, and metal oxide-coated PTCD (2 cycles). b–d) Charge/discharge profile of different metal oxide-coated PTCD at different current rates.

samples gradually decrease with an increase in the current density due to the low diffusion rate of the Na^+ ions into the PTCD electrodes. However, all metal oxide-coated PTCD materials exhibit discharge capacities higher than that of the uncoated PTCD, indicating an enhancement in Na^+ diffusion into the active material after the deposition of the coating layer. The coating layer can significantly reduce the interface resistance and provide more channels for Na^+ diffusion, thereby elevating the kinetics of PTCD.[54] Among the three metal oxides, Ti-PTCD exhibited considerably improved capacity retention at high current rates compared to pristine PTCD. The rate performance of PTCD increases in the following order: pristine < ZnO < Al_2O_3 < TiO_2. A discharge capacity of ≈91, 82, 77, and 70 mAh g^{-1} was delivered at 10 A g^{-1} (71C) by Ti-PTCD, Al-PTCD, Zn-PTCD, and pristine PTCD, respectively. The rate performance of the PTCD is primarily influenced by the conductivity of its coating layer. The bandgap energies of TiO_2, ZnO, and Al_2O_3 are ≈3.2, 3.37, and 7.2 eV, respectively; electrons from the cathode can easily reach the coating material with a low bandgap energy. A low bandgap energy in TiO_2 can easily facilitate the electron movement in Ti-PTCD, thereby achieving a high rate capability. Although the bandgap of Al_2O_3 is higher than ZnO, the sodiated $Na_xAl_2O_3$ formed during the initial cycling could improve the kinetics of Al-PTCD during the later cycles.[53] To further investigate the effect of the coatings, electrochemical impedance spectra (EIS) were recorded for all PTCD samples, and the corresponding Nyquist plots are presented in Figure S4a in the Supporting Information. All the metal oxide coatings on PTCD effectively reduced the internal resistance compared to that of pristine PTCD. The charge-transfer resistance (R_{ct}) values show predominant difference after metal oxide coatings. Overall, the highly stable TiO_2 protecting layer on PTCD has effectively decreased the cell resistance, consequently improving the kinetics and stability of the electrode.[55] A uniform and ultrathin TiO_2 coating can greatly reduce the interface resistance between PTCD and electrolyte and improves the kinetics of the redox reaction.

The effect of coating thickness on PTCD is further evaluated. Upon coating with thicker metal oxide films (5 cycles of ALD), the initial discharge capacities and first-cycle Coulombic efficiency of the Ti-PTCD decrease (**Figure 4**a). It is observed that Ti-PTCD (5 cycles) features higher polarization than the Ti-PTCD (2 cycles). The increase in the metal oxide coating beyond the threshold limit is likely to limit the diffusion of Na^+ ion, and impedes the facile movement of Na^+ through the thick metal oxide layer. Thicker coatings hinder the fast movement of sodium ions and reduce the active participation of the electrochemically active PTCD during the initial cycles. However, the Coulombic efficiency and discharge capacity recovers upon consecutive cycles, and reaches ≈99%, and ≈120 mAh g^{-1} respectively. As can be inferred from Figure 4b, thicker metal oxide coatings (5 cycles) have a detrimental effect on the rate performance of PTCD. Although a similar capacity is obtained at low current rates, the capacity of Ti-PTCD (5 cycles) at 71C reaches ≈76 mAh g^{-1}, much closer to pristine PTCD. Upon coating with thicker metal oxide films, the diffusion time for sodium ion scales up, and thereby reducing the kinetics of the Ti-PTCD at high current rate. The Nyquist plots of Ti-PTCD

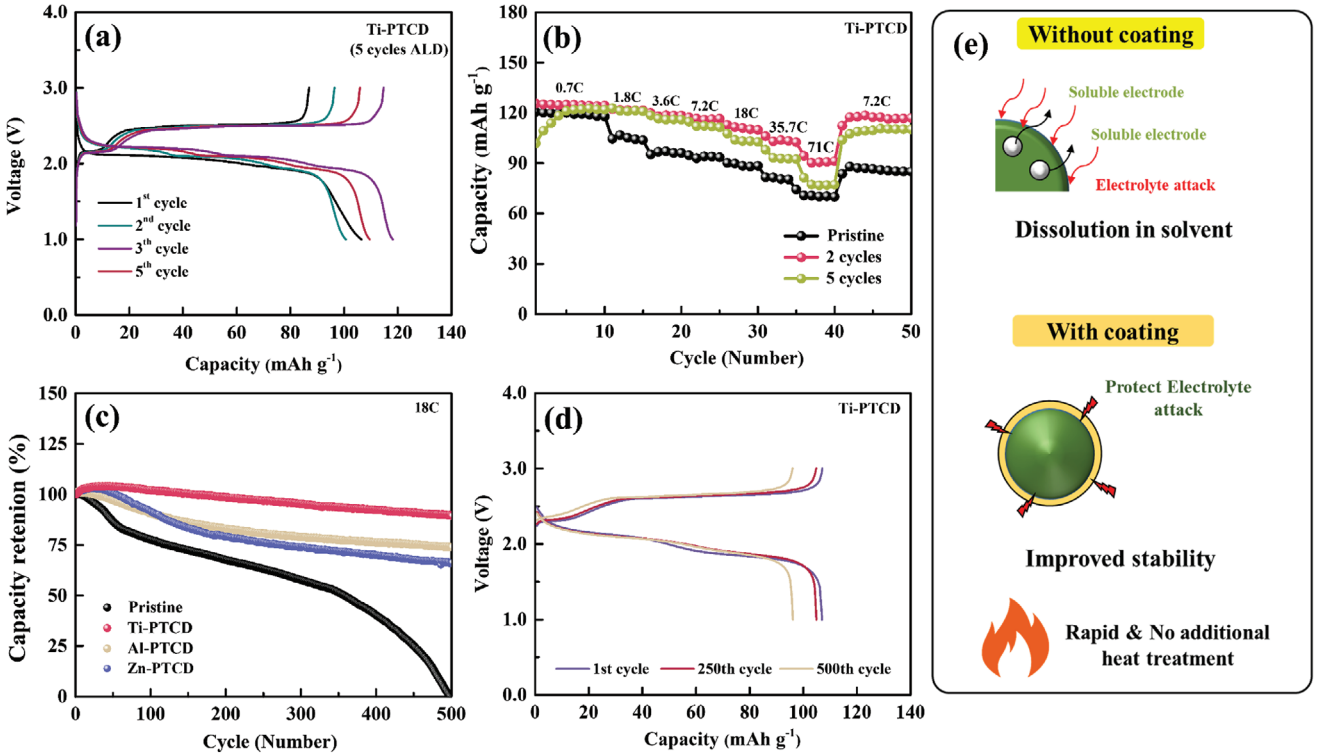

Figure 4. Effect of metal oxide coating thickness: a) Charge/discharge profile of Ti-PTCD (5 cycles) at 0.1 A g^{-1}; b) effect of the TiO_2 coating thickness on the rate performance of PTCD. c) Cyclic stability for different metal oxide-coated (2 cycles) PTCD samples at 18C (2.5 A g^{-1}). d) Charge/discharge profile of Ti-PTCD (2 cycles) during cyclic stability. e) Scheme for the effect of metal oxide coating layer on PTCD.

(5 cycles) in Figure S4b in the Supporting Information shows higher charge-transfer resistance (R_{ct}) than Ti-PTCD (2 cycles). A thicker metal coating on PTCD can considerably hinder the facile Na^+ diffusion at a higher current rate, increase the polarization, and lower the active material utilization. A similar effect is observed for Al-PTCD, and Zn-PTCD with higher coating thickness (Figure S5, Supporting Information). Increasing the coating beyond the threshold value highly impacts the Na^+ diffusion and reduces the discharge capacity at high current rates.[56]

The cyclic stability of PTCD with and without metal oxides was studied at 18C (2.5 A g^{-1}), and the results are presented in Figure 4c. All the metal oxide-coated samples deliver a more stable discharge capacity than pristine PTCD, effectively preventing the dissolution of the organic electrode. Pristine PTCD exhibits a continuous capacity decay upon cycling, and this is attributed to the continuous electrode dissolution in the organic electrolyte medium. However, the presence of the metal oxide interface prevents the direct attack of the electrolyte on the PTCD particles, thereby preventing the electrode dissolution to a great extent. The stability of the metal oxide coating increases in the following order: pristine < ZnO < Al_2O_3 < TiO_2. The pristine sample drastically and fully loses its capacity with cycling, whereas the TiO_2-coated samples retain ≈89% of their capacity after 500 cycles. The cyclic stabilities of Zn-PTCD and Al-PTCD are ≈66% and ≈74%, respectively, lower than that of Ti-PTCD. Figure 4d shows the charge discharge profiles of Ti-PTCD at different cycles, and it can be observed that Ti-PTCD delivered a stable capacity with low polarization after prolonged cycling. Figure 4e depicts the role of the protective metal oxide coating in maintaining the electrochemical stability of organic electrodes. In the absence of a protective layer, PTCD is easily exposed to electrolyte attack, and it undergoes gradual dissolution upon cycling. In contrast, the protective coating prevents the direct contact of the electrolyte and PTCD to enhance the electrochemical performance.[36] Utilizing a rapid coating technique with no additional heat treatment step is an eminent approach to improve the practical capability of organic electrodes. This can also be confirmed from cycled sodium metal anode, where the sodium metal anode using pristine PTCD shows a dark PTCD deposition after cycling, whereas the sodium metal anode using Ti-PTCD shows a brighter nature with no PTCD deposition after cycling (Figure S6, Supporting Information). The pristine PTCD without protective layer can easily dissolute through porous separator and gets deposited over sodium metal, causing severe damage to the cell.[57] However, the metal oxide protective layer can effectively prevent the active material dissolution during cycling process, and prevents the PTCD deposition over sodium metal. Figure S7 in the Supporting Information compares the cyclic stabilities of the PTCD samples coated with 2 and 5 cycles of TiO_2 deposition. Although a higher stability is observed in the case of the Ti-PTCD with a thicker coating (5 cycles), the obtained capacity is lower than that in the case of the Ti-PTCD with thinner coating (2 cycles). The PTCD coated with 5 cycles of TiO_2 exhibits a capacity retention of ≈93% after 500 cycles. This is attributed to the encapsulation of PTCD by the highly dense and thick coating that

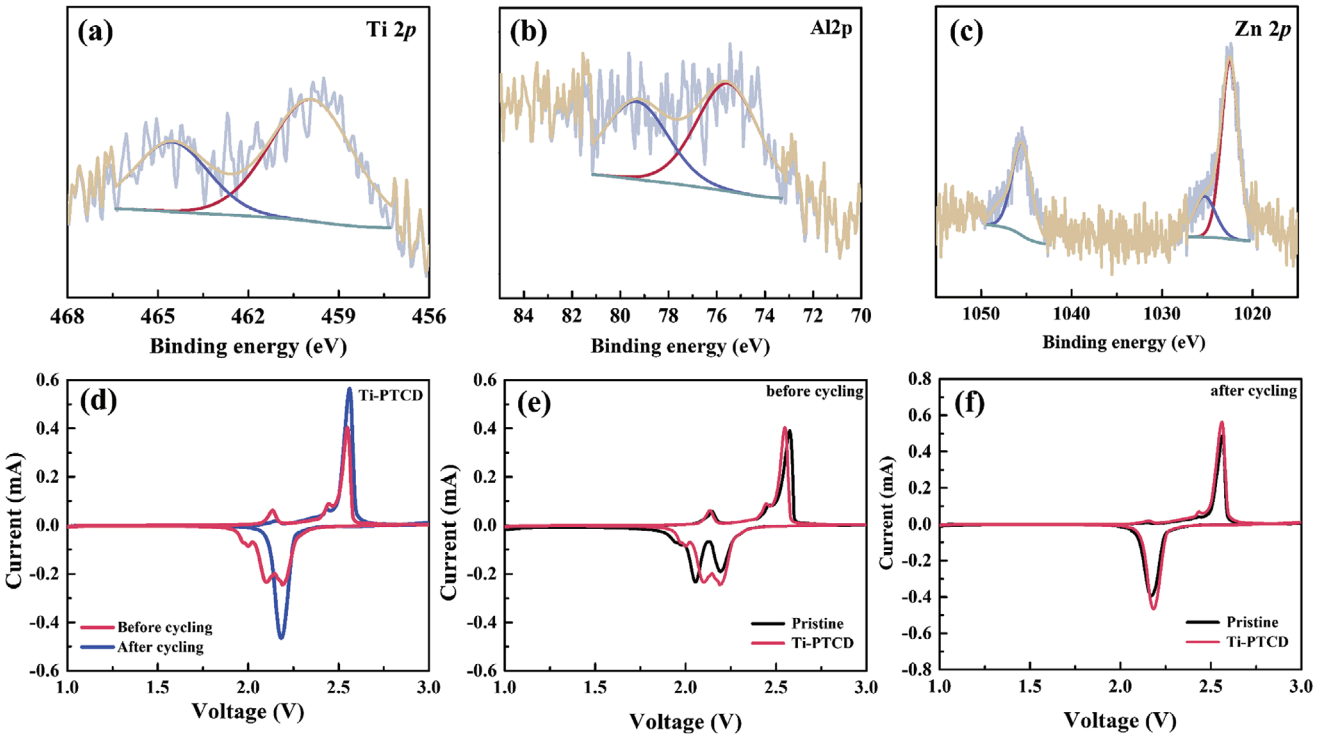

Figure 5. XPS spectra of metal oxide-coated PTCD samples after cycling: a) Ti-PTCD, b) Al-PTCD, and c) Zn-PTCD; CV curves of PTCD after cycling: d) Ti-PTCD, e) pristine and Ti-PTCD before cycling, and f) pristine and Ti-PTCD after cycling.

reduces the PTCD exposure to the electrolyte during cycling. However, such dense coatings are not favorable for achieving high kinetics. Table S1 in the Supporting Information compares the electrochemical performance characteristics of PTCD to those of several other previously reported organic electrodes. It is clearly observed that PTCD electrodes with ultrathin protective coatings exhibit improved kinetics and stability even with low conductive carbon. Thus, this strategy can overcome the problem of volumetric energy density arising from the presence of a large amount of dead conductive carbon. To further elucidate the effect of TiO_2 coating, electrochemical performance of pristine PTCD, and Ti-PTCD without conductive carbon (PTCD:binder = 8:2, weight ratio) is evaluated (Figure S8, Supporting Information). Pristine PTCD without conductive carbon undergoes a near 2 Na^+ reaction during initial cycles, delivering a capacity of ≈90 mAh g^{-1} at 0.1 A g^{-1}. However, the discharge capacity at high rate is too low, and the capacity retention decreases with cycling due to high resistance between the PTCD electrode materials without conductive carbon. Ti-PTCD without conductive carbon delivered a similar capacity as pristine PTCD, and TiO_2 coating do not influence the kinetics. This is mainly due to poor electronic conductivity of PTCD organic electrode that impedes the electron flow between PTCD particles and current collector. However, stability of Ti-PTCD is superior to pristine Ti-PTCD as TiO_2 coating can efficiently prevent the electrolyte dissolution. Conductive carbon network between the organic electrode particles also plays a crucial in achieving a superior rate performance.

The differences in stability between several metal oxide coatings are attributed to the differences in chemical stability between the protective layers and the differences in interactions between the electrode and the Na^+ ions during the electrochemical reaction. XPS analysis was conducted on the metal oxide-coated PTCD to reveal the chemical changes in the metal oxides after cycling. The XPS survey spectra of the coated PTCD samples after cycling (Figure S9, Supporting Information) exhibit signature peaks from the corresponding metal oxides even after the cycling process, indicating the presence of a stable interface layer over the PTCD particles even after prolonged cycling. However, the deconvoluted XPS spectra of metal oxides clearly indicate the change in the chemical nature of PTCD after cycling.

Unlike for other metal oxides, the Ti_{2p} spectrum of Ti-PTCD (**Figure 5**a) was essentially unchanged even after cycling, indicating the robust stability of the TiO_2 coating layer. While it is well known that TiO_2 undergoes Li^+ intercalation at ≈1.5 V versus Li/Li^+ to form $LiTiO_2$, Na^+ ion intercalation in TiO_2 exhibits a different behavior.[58,59] The electrochemically active TiO_2 undergoes reversibly pseudocapacitive Na^+ storage between the working voltage regions (3–1 V vs Na) of PTCD. TiO_2 undergoes a disproportionation reaction with Na^+ only at lower sodiation potentials (<0.5 V vs Na).[60] The chemically stable nature of TiO_2 plays a critical role in preventing the direct electrode–electrolyte interaction that leads to the problematic dissolution of PTCD. The pseudocapacitive interaction of TiO_2 with Na^+ ions is also beneficial for improving the kinetics of PTCD and achieving a high rate performance. While the use of Al_2O_3 coatings proved to be highly successful in LIBs and SIBs and critically improved the stability of several electrode materials,[61,62] Al_2O_3 coatings delivered an inferior performance when employed on organic

electrodes for SIBs. The sodiation of Al_2O_3 is energetically unfavorable during initial cycles, and Al_2O_3 undergoes elastic expansion during the sodiation process. Furthermore, the ClO_4 anions from the electrolyte can interact with the Al_2O_3 coating, so that the electrode undergoes a reduction process. This can be observed from the deconvoluted Al_{2p} spectrum (Figure 5b), where peaks from the organo-aluminum interaction are observed at ≈79.2 eV.[63,64] Similarly, the deconvoluted Zn_{2p} peaks in Figure 5c show the formation of a new peak at 1021.2 eV, corresponding to the Zn(0) metal in Zn-PTCD. A significant amount of electrochemically active ZnO can be irreversibly converted into the Zn metal during the sodiation process. However, the traces from Na–Zn alloy formation were not observed because the formation of this alloy requires a lower sodiation potential.[49] These chemical changes in the metal oxide coating can reduce the stiffness of the protection layer and allow the electrode–electrolyte contact after repeated cycling.

To obtain more insight into the influence of the TiO_2 coating layer on PTCD, cyclic voltammetry (CV) measurements were recorded for pristine PTCD and Ti-PTCD before and after cycling. The CV curves before cycling presented in Figure 5d,e detail the reduced polarization of the redox curves, along with the more narrow potential difference of the anodic and cathodic peaks after TiO_2 coating, indicating a facile electrochemical reaction after coating. Furthermore, for the sample without a protective coating layer, the low-voltage region in CV shows a high decomposition current. The decomposition at a low voltage was highly reduced after the TiO_2 coating layer was deposited, indicating the reduced electrolyte decomposition and a uniform formation of the SEI layer. The two major cathodic peaks present before cycling merge into a single peak in both pristine PTCD and Ti-PTCD due to the chemical change in PTCD that requires further investigation.[40] However, the redox peaks in the anodic scan are clearly visible for Ti-PTCD; the polarization is significantly reduced, and it becomes negligible after the coating process. The CV curves of Al-PTCD and Zn-PTCD after cycling presented in Figure S10 in the Supporting Information exhibit a similar phenomenon, indicating the crucial role of the protective coating in improving the stability of organic electrodes.

3. Conclusion

Understanding the interphase behavior and kinetics in organic molecules is essential for the design of next-generation eco-friendly energy storage devices. We successfully demonstrated that the use of metal oxide coatings deposited by ALD on the perylene-3,4,9,10-tetracarboxylicacid dianhydride organic electrode is a novel approach to realizing organic SIBs with high energy density and stability. A simple and ultrathin metal oxide coating can considerably increase the interphase stability and enhance the Na-ion kinetics of PTCD. Importantly, such high kinetics are achieved in the PTCD electrodes without compromising on the volumetric performance, i.e., with a low conductive carbon content. Moreover, the high capacity and stability achieved after ALD coating are comparable to those of conventional inorganic electrode materials. This coating strategy can overcome the current limitations of organic electrodes such as high electrode dissolution, poor electrochemical kinetics, and high electrochemically inactive carbon content. However, coatings with high chemical stability and favorable properties must be used for the manipulation of organic electrode particles. Similar strategies can be employed for other organic cathodes, paving the way for the realization of high-performance, all-organic SIBs.

4. Experimental Section

Various metal oxides (TiO_2, Al_2O_3, and ZnO) were directly coated on the electrodes in laminar-flow-type ALD thermal reactor (NCD, Lucida D100, Korea). Titanium tetraisopropoxide (TTIP), trimethylaluminum (TMA), and diethylzinc (DEZ) were used as the precursors for Ti, Al, and Zn, respectively, whereas H_2O was used as the oxidizer in all the cases. The precursors obtained from the vendor (Sigma-Aldrich, and Strem chemicals) were used for deposition. The deposition temperature was set as 120, 150, and 150 °C for TiO_2, Al_2O_3, and ZnO, respectively. The deposition cycle of TiO_2, Al_2O_3, and ZnO was carried out using the sequences of 2 (TTIP)–20 (N_2)–1 (H_2O)–20 (N_2), 0.5 (TMA)–20 (N_2)–1 (H_2O)–20(N_2), and 0.5 (DEZ)–20 (N_2)–1 (H_2O)–20 (N_2), respectively. The number of ALD cycles was varied—2, 5, and 50 cycles—to vary the thickness of the coating layer on the electrodes.

Material Characterization: XRD patterns were recorded using a Rigaku Rint 1000 (Japan) diffractometer with Cu Kα radiation. The morphology of the PTCD powders was recorded using field emission scanning electron microscope (FE-SEM, Hitachi S4700) and HR-TEM (TECNAI, Philips, The Netherlands, 200 KeV). XPS was carried out using a MultiLab 2000 spectrometer (Thermo Scientific, UK) with a monochromatized Al Kα X-ray source ($h\nu$ = 1486.71 eV).

Electrochemical Characterization: The electrodes used to examine the half-cell performance of PTCD had the following composition: 70% active material, 15% Super P (conductive carbon), and 15% PVDF binder. The electrode slurry was rolled over a copper foil and then dried at 120 °C overnight in a vacuum oven. The typical mass loading of the electrode was ≈2 mg cm^{-2}. The electrodes were cycled against the sodium foil in the half-cell configuration (CR 2032) with a glass fiber separator and 1 M $NaClO_4$ in polycarbonate as the electrolyte. The coin cells were assembled inside an argon-filled glove box. Cyclic voltammetry and galvanostatic charge/discharge studies were conducted in a Won-A-Tech (WBCS 3000, Korea) battery tester. Electrochemical impedance spectra was performed using a using a Bio-Logic (SP-150, France) electrochemical workstation in the frequency range of 200 kHz to 100 mHz.

Supporting Information

Supporting Information is available from the Wiley Online Library or from the author.

Acknowledgements

This work was supported by the National Research Foundation of Korea (NRF) grant funded by the Korea government (Ministry of Science, ICT & Future Planning) (No. 2019R1A2C1007620). R.T. acknowledges the support from the National Research Foundation of Korea (NRF) grant funded by the Korea government (MSIT) (No. 2020R1C1C1014961).

Conflict of Interest

The authors declare no conflict of Interest.

Keywords

atomic layer deposition, electrode interfaces, metal oxide, organic electrodes, protective coatings

Received: June 17, 2020
Revised: July 25, 2020
Published online: September 22, 2020

[1] J.-Y. Hwang, S.-T. Myung, Y.-K. Sun, *Chem. Soc. Rev.* **2017**, *46*, 3529.
[2] C. Vaalma, D. Buchholz, M. Weil, S. Passerini, *Nat. Rev. Mater.* **2018**, *3*, 18013.
[3] B. Moorthy, J.-H. Kim, H.-W. Lee, D. K. Kim, *Energy Storage Mater.* **2020**, *24*, 602.
[4] Y. You, A. Manthiram, *Adv. Energy Mater.* **2018**, *8*, 1701785.
[5] R. Thangavel, A. G. Kannan, R. Ponraj, X. Sun, D.-W. Kim, Y.-S. Lee, *J. Mater. Chem. A* **2018**, *6*, 9846.
[6] S. Shi, C. Sun, X. Yin, L. Shen, Q. Shi, K. Zhao, Y. Zhao, J. Zhang, *Adv. Funct. Mater.* **2020**, *30*, 1909283.
[7] C. Ding, L. Huang, J. Lan, Y. Yu, W.-H. Zhong, X. Yang, *Small* **2020**, *16*, 1906883.
[8] Y. Fang, L. Xiao, Z. Chen, X. Ai, Y. Cao, H. Yang, *Electrochem. Energy Rev.* **2018**, *1*, 294.
[9] H.-G. Wang, X.-B. Zhang, *Chem. - Eur. J.* **2018**, *24*, 18235.
[10] R. Thangavel, A. G. Kannan, R. Ponraj, G. Yoon, V. Aravindan, D.-W. Kim, K. Kang, W.-S. Yoon, Y.-S. Lee, *Energy Storage Mater.* **2020**, *25*, 702.
[11] X. Yin, S. Sarkar, S. Shi, Q.-A. Huang, H. Zhao, L. Yan, Y. Zhao, J. Zhang, *Adv. Funct. Mater.* **2020**, *30*, 1908445.
[12] Y. Xu, M. Zhou, Y. Lei, *Mater. Today* **2018**, *21*, 60.
[13] C. Wang, R. Chu, Z. Guan, Z. Ullah, H. Song, Y. Zhang, C. Yu, L. Zhao, Q. Li, L. Liu, *Nanoscale* **2020**, *12*, 4729.
[14] T. B. Schon, B. T. McAllister, P.-F. Li, D. S. Seferos, *Chem. Soc. Rev.* **2016**, *45*, 6345.
[15] Q. Zhao, Y. Lu, J. Chen, *Adv. Energy Mater.* **2017**, *7*, 1601792.
[16] W. Deng, Y. Shen, J. Qian, Y. Cao, H. Yang, *ACS Appl. Mater. Interfaces* **2015**, *7*, 21095.
[17] F. Xu, H. Wang, J. Lin, X. Luo, S.-a. Cao, H. Yang, *J. Mater. Chem. A* **2016**, *4*, 11491.
[18] M. Lee, J. Hong, J. Lopez, Y. Sun, D. Feng, K. Lim, W. C. Chueh, M. F. Toney, Y. Cui, Z. Bao, *Nat. Energy* **2017**, *2*, 861.
[19] X. Han, C. Chang, L. Yuan, T. Sun, J. Sun, *Adv. Mater.* **2007**, *19*, 1616.
[20] K. Sakaushi, E. Hosono, G. Nickerl, T. Gemming, H. Zhou, S. Kaskel, J. Eckert, *Nat. Commun.* **2013**, *4*, 1485.
[21] A. Iordache, V. Delhorbe, M. Bardet, L. Dubois, T. Gutel, L. Picard, *ACS Appl. Mater. Interfaces* **2016**, *8*, 22762.
[22] L. Fédèle, F. Sauvage, M. Bécuwe, *J. Mater. Chem. A* **2014**, *2*, 18225.
[23] H. Banda, D. Damien, K. Nagarajan, A. Raj, M. Hariharan, M. M. Shaijumon, *Adv. Energy Mater.* **2017**, *7*, 1701316.
[24] Y. Lu, Q. Zhang, L. Li, Z. Niu, J. Chen, *Chem* **2018**, *4*, 2786.
[25] J. Xie, Q. Zhang, *J. Mater. Chem. A* **2016**, *4*, 7091.
[26] Y. Chen, W. Luo, M. Carter, L. Zhou, J. Dai, K. Fu, S. Lacey, T. Li, J. Wan, X. Han, Y. Bao, L. Hu, *Nano Energy* **2015**, *18*, 205.
[27] Y. Wang, Y. Ding, L. Pan, Y. Shi, Z. Yue, Y. Shi, G. Yu, *Nano Lett.* **2016**, *16*, 3329.
[28] X. Wu, S. Jin, Z. Zhang, L. Jiang, L. Mu, Y.-S. Hu, H. Li, X. Chen, M. Armand, L. Chen, X. Huang, *Sci. Adv.* **2015**, *1*, e1500330.
[29] J. Xie, P. Gu, Q. Zhang, *ACS Energy Lett.* **2017**, *2*, 1985.
[30] R. Thangavel, R. Ponraj, A. G. Kannan, K. Kaliyappan, D. W. Kim, Z. Chen, Y.-S. Lee, *Green Chem.* **2018**, *20*, 4920.
[31] S. Lee, G. Kwon, K. Ku, K. Yoon, S.-K. Jung, H.-D. Lim, K. Kang, *Adv. Mater.* **2018**, *30*, 1704682.
[32] B. Häupler, A. Wild, U. S. Schubert, *Adv. Energy Mater.* **2015**, *5*, 1402034.
[33] H. Kim, J. E. Kwon, B. Lee, J. Hong, M. Lee, S. Y. Park, K. Kang, *Chem. Mater.* **2015**, *27*, 7258.
[34] Z. Song, H. Zhou, *Energy Environ. Sci.* **2013**, *6*, 2280.
[35] Y. Liu, X.-J. Lin, Y.-G. Sun, Y.-S. Xu, B.-B. Chang, C.-T. Liu, A.-M. Cao, L.-J. Wan, *Small* **2019**, *15*, 1901019.
[36] K. R. Adair, C. Zhao, M. N. Banis, Y. Zhao, R. Li, M. Cai, X. Sun, *Angew. Chem.* **2019**, *58*, 15797.
[37] Y. Zhong, X. Xia, S. Deng, J. Zhan, R. Fang, Y. Xia, X. Wang, Q. Zhang, J. Tu, *Adv. Energy Mater.* **2018**, *8*, 1701110.
[38] J. Dai, C. Yang, C. Wang, G. Pastel, L. Hu, *Adv. Mater.* **2018**, *30*, 1802068.
[39] S. Xu, D. W. McOwen, C. Wang, L. Zhang, W. Luo, C. Chen, Y. Li, Y. Gong, J. Dai, Y. Kuang, C. Yang, T. R. Hamann, E. D. Wachsman, L. Hu, *Nano Lett.* **2018**, *18*, 3926.
[40] R. Thangavel, K. Kaliyappan, D.-U. Kim, X. Sun, Y.-S. Lee, *Chem. Mater.* **2017**, *29*, 7122.
[41] K. Kaliyappan, J. Liu, A. Lushington, R. Li, X. Sun, *ChemSusChem* **2015**, *8*, 2537.
[42] X. Fan, C. Luo, J. Lamb, Y. Zhu, K. Xu, C. Wang, *Nano Lett.* **2015**, *15*, 7650.
[43] W. Ai, W. Zhou, Z. Du, C. Sun, J. Yang, Y. Chen, Z. Sun, S. Feng, J. Zhao, X. Dong, W. Huang, T. Yu, *Adv. Funct. Mater.* **2017**, *27*, 1603603.
[44] C. Wang, W. Tang, Z. Yao, B. Cao, C. Fan, *Chem. Commun.* **2019**, *55*, 1801.
[45] Z. Xing, Z. Jian, W. Luo, Y. Qi, C. Bommier, E. S. Chong, Z. Li, L. Hu, X. Ji, *Energy Storage Mater.* **2016**, *2*, 63.
[46] S. Kalluri, M. Yoon, M. Jo, H. K. Liu, S. X. Dou, J. Cho, Z. Guo, *Adv. Mater.* **2017**, *29*, 1605807.
[47] R. Thangavel, B. Moorthy, D. K. Kim, Y.-S. Lee, *Adv. Energy Mater.* **2017**, *7*, 1602654.
[48] R. Thangavel, A. G. Kannan, R. Ponraj, M.-S. Park, H. Choi, D.-W. Kim, Y.-S. Lee, *Adv. Mater. Interfaces* **2018**, *5*, 1800472.
[49] S. Sinha, P. N. Didwal, D. K. Nandi, J. Y. Cho, S.-H. Kim, C.-J. Park, J. Heo, *Ceram. Int.* **2019**, *45*, 1084.
[50] W. Luo, M. Allen, V. Raju, X. Ji, *Adv. Energy Mater.* **2014**, *4*, 1400554.
[51] J. Kasnatscheew, M. Evertz, B. Streipert, R. Wagner, R. Klöpsch, B. Vortmann, H. Hahn, S. Nowak, M. Amereller, A. C. Gentschev, P. Lamp, M. Winter, *Phys. Chem. Chem. Phys.* **2016**, *18*, 3956.
[52] M. Gauthier, T. J. Carney, A. Grimaud, L. Giordano, N. Pour, H.-H. Chang, D. P. Fenning, S. F. Lux, O. Paschos, C. Bauer, F. Maglia, S. Lupart, P. Lamp, Y. Shao-Horn, *J. Phys. Chem. Lett.* **2015**, *6*, 4653.
[53] S. C. Jung, H.-J. Kim, J. W. Choi, Y.-K. Han, *Nano Lett.* **2014**, *14*, 6559.
[54] X. Fang, F. Lin, D. Nordlund, M. Mecklenburg, M. Ge, J. Rong, A. Zhang, C. Shen, Y. Liu, Y. Cao, M. M. Doeff, C. Zhou, *Adv. Funct. Mater.* **2017**, *27*, 1602873.
[55] C. Wang, Y. Fang, Y. Xu, L. Liang, M. Zhou, H. Zhao, Y. Lei, *Adv. Funct. Mater.* **2016**, *26*, 1777.
[56] X. Li, J. Liu, X. Meng, Y. Tang, M. N. Banis, J. Yang, Y. Hu, R. Li, M. Cai, X. Sun, *J. Power Sources* **2014**, *247*, 57.
[57] R. L. Belanger, B. Commarieu, A. Paolella, J.-C. Daigle, S. Bessette, A. Vijh, J. P. Claverie, K. Zaghib, *Sci. Rep.* **2019**, *9*, 1213.
[58] H. Kim, M.-Y. Cho, M.-H. Kim, K.-Y. Park, H. Gwon, Y. Lee, K. C. Roh, K. Kang, *Adv. Energy Mater.* **2013**, *3*, 1500.
[59] Q. Wu, Y. Yin, S. Sun, X. Zhang, N. Wan, Y. Bai, *Electrochim. Acta* **2015**, *158*, 73.
[60] Z. Le, F. Liu, P. Nie, X. Li, X. Liu, Z. Bian, G. Chen, H. B. Wu, Y. Lu, *ACS Nano* **2017**, *11*, 2952.
[61] P. Yan, J. Zheng, X. Zhang, R. Xu, K. Amine, J. Xiao, J.-G. Zhang, C.-M. Wang, *Chem. Mater.* **2016**, *28*, 857.
[62] J.-Y. Hwang, S.-T. Myung, J. U. Choi, C. S. Yoon, H. Yashiro, Y.-K. Sun, *J. Mater. Chem. A* **2017**, *5*, 23671.
[63] M. A. Amin, *Electrochim. Acta* **2009**, *54*, 1857.
[64] L. D. Atanasoska, D. M. Dražić, A. R. Despić, A. Zalar, *J. Electroanal. Chem. Interfacial Electrochem.* **1985**, *182*, 179.